Proceedings of the ASME 2010 3rd Joint US-European Fluids Engineering Summer Meeting and 8th International Conference on Nanochannels, Microchannels, and Minichannels
FEDSM-ICNMM2010
August 1-5, 2010, Montreal, Canada

FEDSM-ICNMM2010-30535

A STUDY ON FLOW THROUGH A PERIODIC ARRAY OF POROUS MEDIUM CYLINDERS BY IMMERSED-BOUNDARY METHODS

Xiaofan Yang
Mechanical and Nuclear Engineering
Kansas State University, Manhattan, KS, USA
xiaofan@ksu.edu

Zhongquan Charlie Zheng *
Mechanical and Nuclear Engineering
Kansas State University, Manhattan, KS, USA
zzheng@ksu.edu

Ying Xu
Mechanical and Nuclear Engineering
Kansas State University, Manhattan, KS, USA
yingxu@ksu.edu

ABSTRACT

Numerical simulations with an immersed-boundary method are presented for the incompressible flow past a periodic array of porous-medium cylinders. Fluid/porous-medium interactions are greatly influenced by the accuracy on the interface between the surface of the porous cylinder and the flow around it, because of the sudden change in the governing equations for the fluid and for the porous material. In order to retain the smoothness on the interface, momentum fluxes near the interface are discretized using several schemes, including the 2nd- and 3rd-order upwind schemes and the 5th-order Weighted Essentially Non-Oscillatory (WENO) scheme. These schemes are combined with a direct-forcing immersed-boundary method to remove the discontinuity between the fluid and the porous material, and thus accuracy near the interface can be improved. Low and moderate Reynolds number flows, both outside and inside the porous cylinders, are computed simultaneously by solving a combined governing equation set for incompressible flow. The simulation is first validated using flow over an array of impermeable cylinders. The advantage of high-order schemes is then investigated by looking at the flow parameters near the interfaces between the porous cylinders and the outside flow. Species transport in flow with the porous-cylinder-array configuration is also studied.

INTRODUCTION

Flow past cylinders has been extensively investigated for decades. This fundamental problem can be applied to various industrial structures, such as off-shore constructions, heat exchangers, etc. Both experimental and numerical methods were used to study this problem. Different flow Reynolds numbers and cylinder shapes and their arrangements have been tested for various objectives. The review of flow over a single circular cylinder can be found in, e.g., Williamson (1996) and Zdravkovich (1997). To study multi-body fluid/solid interactions, tandem cylinder configurations have been studied (e.g., Papaioannou 2006a, 2006b, and Yang and Zheng, 2010). Staggered cylinder bundles draw some attentions in recent years, as the complicated structures are challenging to simulate fluid/structure interactions (FSI). Rollet-Miet *et al.* (1999) used Large Eddy Simulation (LES) to study turbulent flow past a cylinder bank. The instantaneous flow field and Reynolds stress components were calculated. For fluid flowing through porous materials, multiple-cylinder structures can be viewed as a representative elementary volume (REV) to study the fluid flow in micro-scales. In Kuwahara *et al.* (1998, 2006), a square cylinder REV was used to study the macroscopic fluid transport phenomena from the microscopic approach in a range of Reynolds numbers and porosities. LES was also applied for high Reynolds number cases in that study. The correlation between the pressure gradient and the porous properties was analyzed and compared to the macroscopic analytical solution. The good agreement in the comparison proved the validity of using the REV approach to study flow in porous media. Other works in the literature studied the cylinder bundle problem for either heat exchangers or porous media, including Pedras *et al.* (2001), Roychowdhury *et al.* (2002), Nakayama *et al.* (2004), Moulinec *et al.* (2004), Liang and Papadakis (2007) and Teruel *et al.* (2007, 2009 a, b, c).

While the staggered cylinder array has been confirmed to be an acceptable REV structure to study flow through porous media in the literature, the cylinders in their study were impermeable and treated as solid bodies. To simulate porous materials composed of pellets made of nano-porous particles,

the porous effect in even smaller scales need to be included. For that purpose, in this study, we further model the cylinders as a porous medium with smaller pores. This concept of using the same REV with and without the porous model is illustrated in Fig. 1.

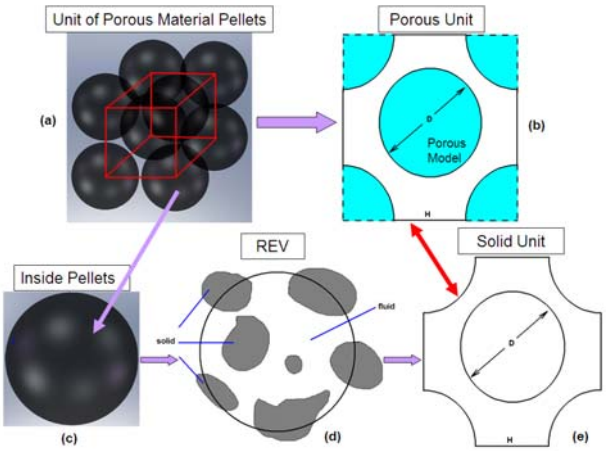

Figure 1 Porous medium REVs represented by fluid/solid-cylinder and fluid/porous-cylinder interactions.

The Darcy or extended Darcy type models can be used as the governing equations in the porous area. In the literature, even the list of studies of flow past a single porous cylinder is much shorter than that for a solid cylinder. For example, Bhattacharyya *et al*. (2006) investigated numerically the flow through and around a porous cylinder, and compared the drag coefficient with the experimental data in flow of a low Reynolds number range (*Re* = 1 - 40). Another example is Chen *et al*. (2008, 2009) who studied the flow past a porous square/trapezoidal cylinder with different Reynolds numbers, Darcy numbers, and porosities. Wilson *et al*. (2006, 2007) applied a simplified and modified porous model, the Zwikker-Kosten (ZK) equation (Zwikker-Kosten, 1949), for time-domain modeling of sound propagation with a porous surface. Recently Xu *et al*. (2010) used the immersed-boundary (IB) method and the ZK equation to study the effect on wind noise reduction of porous windscreens of measurement microphones under different frequencies of incoming wind turbulence. In the current study, we extended the application of the ZK equation to a periodic array of porous cylinders to study momentum transport. We also developed a porous-medium model to calculate mass transport through the array.

The presence of porous media introduces a sudden change (or a discontinuity) at the fluid/porous interface and also affects the numerical stability. Under these circumstances, most conventional finite difference schemes are challenged when used around the interfaces. The accuracy at the interface between the fluid flow and the porous medium is a key issue in simulating such problems (James and Davis, 2001; Goyeau *et al*., 2003). There have been two types of methods to overcome this discontinuity. One is to apply a stress-jump condition between the two media (Ochoa-Tapia and Whitaker, 1995 a, b). In this method, the adjustable parameters that account for the stress jump are critical and problem dependent. Another effective way is to apply higher-order schemes including the 2nd- and 3rd-order upwind schemes and the 5th-order Weighted Essentially Non-Oscillatory (WENO) scheme (Harten *et al*., 1987; Shu and Osher, 1988, 1989). High-order schemes have been used in simulation for viscous flow around steady and moving solid bodies (Cho *et al*. 2007). Also in Xu *et al*. (2010), several high-order schemes were applied on the interfaces between the screened microphone and the outside flow and achieved very promising results.

In the following of the paper, first, the computational schemes were validated by using the solid cylinder REV cases in comparison with the results from a commercial flow solver. Second, flow in the same REV but with the porous model for permeable cylinders is simulated. Different numerical schemes are tested on the fluid/porous interfaces. Then, species transport in the porous medium is studied; and finally conclusions are made.

NUMERICAL SCHEMES

The geometry for both solid and porous REV is shown in Fig. 2 with a periodic array of circular cylinders. In the solid unit, all the cylinders are considered to be impermeable, while in the porous unit, the cylinders are porous. The geometry is determined by two lengths of the unit: the diameter of the cylinder (D) and the distance (H) between the adjacent centers of two cylinders. With this REV unit, the computational domain, including all the related boundary conditions, ensures the periodicity of flow in both the x- and y-directions. Under most circumstances of interest, flow inside porous media is of low speed, therefore laminar, low Reynolds number flows are considered in this study, where $\mathrm{Re} = \rho UD/\mu$, is based on the fluid density ρ, viscosity μ, cylinder diameter D, and the incoming stream velocity U. For the arrangement of the REV in this study, the porosity for the large structure (not inside the cylinder), defined as $\phi = 1-(D/H)^2$, is selected as 0.609375.

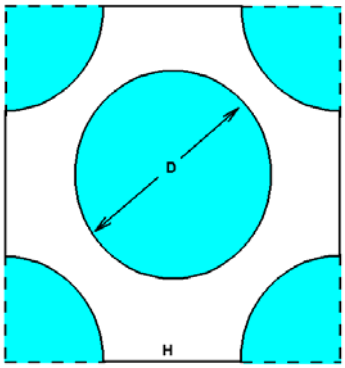

Figure 2 Computational domain of a representative unit structure.

The concept of immersed-boundary (IBM) methods is to implement a defined forcing term in the momentum transport equations in the vicinity of the solid boundary. It has been

successfully used to study various fluid-structure interaction (FSI) problems. The advantages of using IB methods are primarily: 1) only simple Cartesian grid is needed; 2) no moving grid is required to simulate an object in motion; and 3) the shape/arrangement of the objects can be arbitrary. A review of the IB methods can be found in Mittal and Iaccarino (2005). In the current study, a modified immersed-boundary method with a direct compensation forcing term is used to compute the fluid flow. This computational algorithm has been verified using numerous sets of data in the literature on flow over cylinders and spheres (Zhang and Zheng, 2007). The non-dimensional governing equations for the mass and momentum conservations (characterized by the incoming fluid velocity U and the density ρ) for incompressible flow are expressed as:

$$\nabla \cdot \mathbf{u} = 0 \tag{1}$$

and

$$\frac{\partial \mathbf{u}}{\partial t} + \mathbf{u} \cdot \nabla \mathbf{u} = -\nabla p + \frac{1}{Re} \nabla^2 \mathbf{u} + \mathbf{f} \tag{2}$$

where Re is the Reynolds number and $\mathbf{f}$ is the body force representing the virtual boundary or the porous medium effect, which will be defined later.

To include the porous medium effect, Darcy's law has been widely used to simulate the pressure loss (∇p) in the porous medium. Assuming an isotropic medium, Darcy's equation can be written as:

$$\nabla p = -\frac{\mu}{K} \mathbf{u} \tag{3}$$

where μ is the viscosity and K the permeability.

There are several extended formats of Eq. (3). The Zwikker-Kosten (ZK) model has been used previously for numerical calculations of linear sound propagations in porous media (Wilson *et al*., 2006; Xu *et al*., 2010). A modified version of the ZK equation can be written as:

$$\frac{\partial \mathbf{u}}{\partial t} + \mathbf{u} \cdot \nabla \mathbf{u} = -\nabla p + \frac{1}{\mathrm{Re}} \nabla^2 \mathbf{u} - \sigma \mathbf{u} \tag{4}$$

where σ is the dimensionless flow resistivity of the porous medium (non-dimensionalized by $\rho U/D$).

It is obvious that Eqs. (2) and (4) have similar format except for the additional source terms on the right-hand side. Hence in this study, inside the porous medium, a ZK type of source term is applied as the replacement of the forcing term in Eq. (2). The forcing term in the two equations can thus be combined as:

$$\mathbf{f} = \begin{cases} 0 & \text{outside porous medium} \\ -\sigma \mathbf{u} & \text{inside porous medium} \end{cases} \tag{5}$$

After a periodically stable flow field has been obtained, a species transport equation for a passive scalar is solved. Similar to the momentum equation in a porous medium, an additional sink term is needed in the species transport equation to represent the porous effect of the porous cylinders. Thus the species transport equation can be expressed as:

$$\frac{\partial C}{\partial t} + \mathbf{u} \cdot \nabla C = D_c \nabla^2 C + S_c \tag{6}$$

where C is the specie concentration, D_c the species diffusion coefficient, and S_c the additional sink term.

The sink term can be modeled as a simple linearized source:

$$S_c = \begin{cases} 0 & \text{outside the porous medium} \\ -\alpha (C - C_{in}) & \text{inside the porous medium} \end{cases} \tag{7}$$

where α is the absorbing coefficient and C_{in} the final saturated concentration value of the species.

The momentum and species transport equations are solved using finite difference schemes on a staggered Cartesian grid. A semi-implicit scheme with 2nd-order spatial differencing is used for the diffusion terms, with the normal direction diffusion terms being the Crank-Nicholson scheme. The convection terms in both momentum and species transport equations will be discussed later using different orders of schemes. The incompressibility condition is satisfied by solving a Poisson equation for pressure correction using FISHPACK (Swarztrauber and Sweet, 1979). The overall accuracy of the scheme is able to reach the second order in space. More detailed explanations on the IB solver can be found in Zhang and Zheng (2007).

As shown in Fig. 1, there are multiple fluid/porous interfaces in the REV unit. As stated previously, the sudden change between the fluid and the porous medium decreases simulation accuracy. To improve the accuracy near the interfaces, higher-order finite difference schemes are considered. The schemes tested here include the 2nd- and 3rd-order upwind schemes and the 5th-order WENO scheme.

Upwind schemes use an adaptive finite difference stencil to numerically follow the direction of propagation of information. A 1st-order upwind scheme is considered to be too dissipative. Our investigation starts from the 2nd-order. To outline the 2nd-order scheme in this study, consider a simplified 1D wave equation:

$$\frac{\partial u}{\partial t} + a \frac{\partial u}{\partial x} = 0 \tag{8}$$

For the 2nd-order upwind scheme, the discretization of the second term in Eq. (8) is expressed as:

$$\begin{aligned} a \frac{\partial u}{\partial x}\bigg|_{x=x_i^n} &= \max(a,0) \frac{3u_i - 4u_{i-1} + u_{i-2}}{2\Delta x} \\ &+ \min(a,0) \frac{-u_{i+2} + 4u_{i+1} - 3u_i}{2\Delta x} \end{aligned} \tag{9}$$

Similarly, for the 3rd –order upwind scheme, the convective term becomes:

$$\begin{aligned} a \frac{\partial u}{\partial x}\bigg|_{x=x_i^n} &= \max(a,0) \frac{2u_{i+1} + 3u_i - 6u_{i-1} + u_{i-2}}{6\Delta x} \\ &+ \min(a,0) \frac{-u_{i+2} + 6u_{i+1} - 3u_i - 2u_{i-1}}{6\Delta x} \end{aligned} \tag{10}$$

The WENO schemes were developed using a convex combination of all candidate stencils. The 5th -order WENO scheme has a more complicated structure. Consider the same 1D wave equation but in the conservative form:

$$\frac{\partial u}{\partial t}+\frac{\partial q(u)}{\partial x}=0 \tag{11}$$

The derivative of any flux q at the location x_i is discretized as:

$$\left.\frac{\partial q}{\partial x}\right|_{x=x_i}=q_{x,i}=\frac{\hat{q}_{i+1/2}-\hat{q}_{i-1/2}}{\Delta x} \tag{12}$$

If $\partial q/\partial u \geq 0$,

$$\begin{aligned}\hat{q}^{+}_{i+1/2}=&\omega_1(\frac{1}{3}q_{i-2}-\frac{7}{6}q_{i-1}+\frac{11}{6}q_i)\\&+\omega_2(-\frac{1}{6}q_{i-1}+\frac{5}{6}q_i+\frac{1}{3}q_{i+1})\\&+\omega_3(\frac{1}{3}q_i+\frac{5}{6}q_{i+1}-\frac{1}{6}q_{i+2})\end{aligned} \tag{13}$$

where $\omega_j=\dfrac{\alpha_j}{\sum_{k=1}^{3}\alpha_k}$, $\alpha_k=\dfrac{d_k}{(\varepsilon+\beta_k)^2}$, $\varepsilon=10^{-6}$,

$$d_1=\frac{1}{10},\qquad d_2=\frac{3}{5},\qquad d_3=\frac{3}{10},$$

$$\beta_1=\frac{13}{12}(q_{i-2}-2q_{i-1}+q_i)^2+\frac{1}{4}(q_{i-2}-4q_{i-1}+3q_i)^2$$

$$\beta_2=\frac{13}{12}(q_{i-1}-2q_i+q_{i+1})^2+\frac{1}{4}(q_{i-1}-4q_{i+1})^2$$

$$\beta_3=\frac{13}{12}(q_i-2q_{i+1}+q_{i+2})^2+\frac{1}{4}(3q_i-4q_{i+1}+q_{i+2})^2$$

More details on the WENO scheme can be found in Harden et al. (1987), Shu and Osher (1988, 1989) and Cho et al. (2007).

To produce the periodicity in this unit with a length L, periodic boundary conditions have to be enforced in both streamwise and spanwise directions (Patankar et al., 1977) respectively as:

$$u(0,j)=u(L,j),\ \ v(0,j)=v(L,j),\ \ p(0,j)=p(L,j)+\Delta p \tag{14}$$

$$u(i,0)=u(i,L),\ \ v(i,0)=v(i,L),\ \ p(i,0)=p(i,L) \tag{15}$$

For the species transport, the boundary condition at the inlet is chosen to be uniform. The top and bottom boundaries are symmetry, and at the outlet the normal derivatives are zero.

After the grid-size independence check, the grid size, with $dx = dy = 0.00625$, has been chosen for a uniform Cartesian grid. The stability criterion is no more restrictive than that of an explicit scheme for a two-dimensional convection-diffusion equation:

$$\delta t<\min\left[\frac{h^2\,\mathrm{Re}}{4},\frac{2}{(u^2+v^2)\,\mathrm{Re}}\right] \tag{16}$$

where h is the grid size, and u and v are the x- and y-direction velocity components. The first restriction in the minimum function is for diffusion and the second restriction is for convection.

RESULTS AND DISCUSSION

We test several different orders of numerical schemes, and the final selection will go to the scheme which shows the best results among all the cases. We first validate the high-order schemes by comparing the solid cylinder bundle results with the ones calculated using a commercial solver. Second, the porous cylinder unit cases are presented to emphasize the importance of using higher-order schemes. Finally, the results from the species transport will be discussed.

A. Solid cylinder cases

For the solid cylinder cases, the fluid/solid interaction problem in this unique structure is already interesting and is selected to be the validation case before the porous model is involved. By using a commercial CFD solver, the boundary conditions are kept the same as in the IB simulation, including the periodicity and the pressure drop in the streamwise direction. Also the grid resolution is the same between the two simulations. The 2nd-order upwind scheme is used to discretize the convection terms in the commercial solver. The results in Fig. 3(a) and Fig. 3(b) visually show that the velocity field obtained from the IB simulation using the 5th–order WENO scheme and that from the commercial solver look very similar to each other (as the contour scale and levels are kept the same). Higher velocity appears in the narrow channel-like space between the neighbor cylinders. The periodic flow pattern is well represented. Although not shown here, the plots from other schemes look the same as the two shown here.

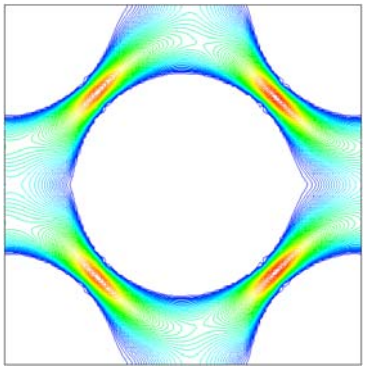

(a)

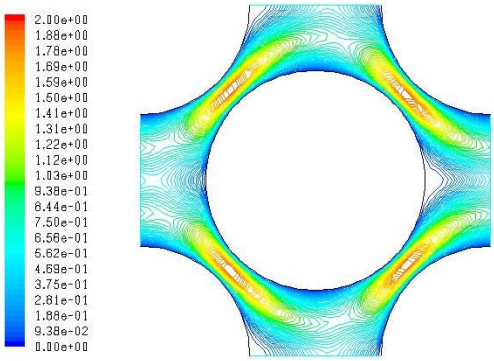

(b)

Figure 3 Velocity magnitude contours for the solid cylinder case: a) 5th-order WENO scheme with IBM; b) the commercial solver simulation (the color range and levels are the same for both cases)

To obtain more strict quantitative comparisons for the results, we select three locations for velocity profile comparisons: the outlet boundary, the top boundary, and along a line in the x-direction which is 1/4 D distance from the bottom of the domain. Results from different schemes are displayed in Fig. 4 and compared with the commercial solver results. In all the locations, the results from 3rd-order upwind scheme and the 5th-order WENO scheme are very close to the commercial solver results, while the results from the two 2nd-order schemes are not. The 2nd-order central difference scheme seems to be the least accurate. We thus decide that the 2nd-order schemes are not the right option even for the solid cylinder case. The 3rd-order upwind and the 5th-order WENO schemes can be the candidates, with the latter showing the best result.

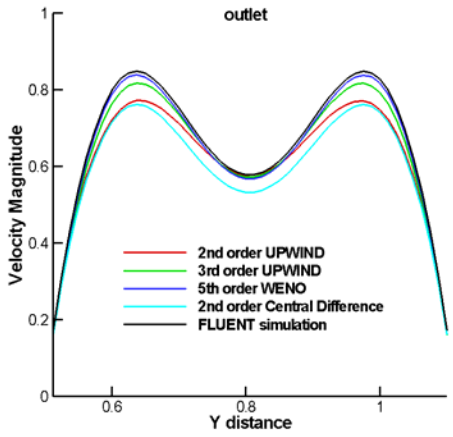

(a) outlet

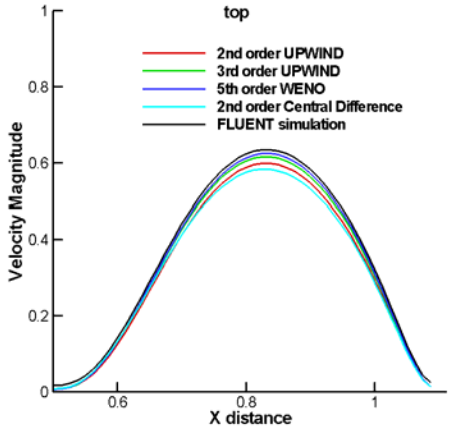

(b) top

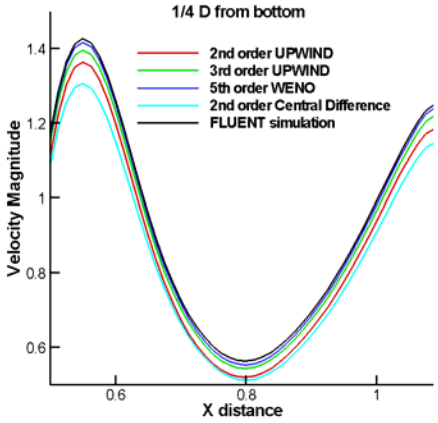

(c) bottom

Figure 4 Velocity profile comparisons for the solid cylinder case among different schemes of IB simulation and the commercial simulation, at three different locations: a) at the outlet; b) at the top boundary; c) 1/4 D from the bottom boundary.

As mentioned in the introduction, the periodic array of solid cylinders is viewed as a representative elementary volume (REV) in a porous medium. The simulation of the flow ion REV can be used as a microscopic representation of flow in the porous medium in order to estimate the macroscopic properties of the porous medium flow. In a macroscopic (or bulk) simulation, the pressure drop is frequently used as the parameter indicating the porous medium behavior. There is the Ergun equation (Ergun, 1952) which relates the pressure drop to the bulk porous medium properties, such as pore size and void fraction. This relationship should also be valid in the micro-scale REV as well. To demonstrate that point, a series of numerical simulations are performed for a range of porosities (ϕ). We then process the microscopic numerical results to compare with the Ergun equation.

To determine the pressure drop (pressure gradient) in an REV, the dimensionless pressure difference between the inlet and the outlet is calculated as (Kuwahara et al., 1998):

$$\frac{dp}{dx} = -\frac{1}{H(H-D/2)} \int_{D/2}^{H-D/2} (p|_{x=0} - p|_{x=H}) dy \qquad (17)$$

The porosities and related pressure gradient calculation results are summarized in Table 1.

ϕ	$(1-\phi)^2/\phi^3$	$-dp/dx$
0.5435	1.298	1.823
0.609375	0.674	1.042
0.75	0.148	0.211
0.826	0.0537	0.051

Table 1 Relationship between the porosity and the pressure gradient

A coefficient of the correlation from current simulations between the dimensionless pressure gradient and $(1-\phi)^2/\phi^3$ is around 142.8 (1.428/0.01, 0.01 is the viscosity μ since Re = 100), which is very close to 144 for circular rods in Kuwahara et al. (1998). Therefore, for laminar flow going through this solid structural unit (a periodic array of impermeable cylinders), the pressure drop can be correlated with the porosity as:

$$-\frac{dp}{dx}=\frac{142.8\mu(1-\phi)^2}{\phi^3 D^2}u \tag{18}$$

This relationship is plotted in Fig. 5. Equation (18) is very close to the empirical expression of the Ergun equation, which is:

$$-\frac{dp}{dx}=\frac{150\mu(1-\phi)^2}{\phi^3 D^2}u \tag{19}$$

The only difference is the coefficient. This coefficient is dependent on the shape of the solid obstacle in the unit.

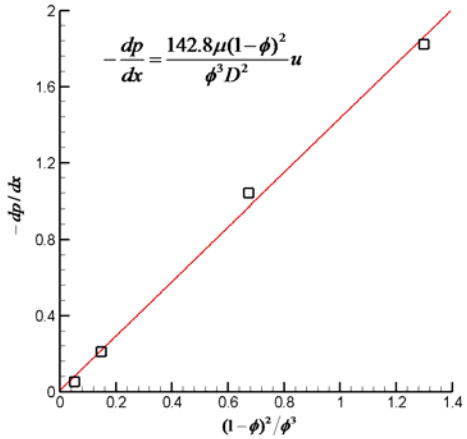

Figure 5 Effect of porosity on pressure gradient

B. Porous cylinder cases

By using the modified ZK equation (Eq. 5) inside the cylinders, flow through porous cylinders can be simulated. A range of flow resistivity values, σ, have been chosen from 0.01 to 10000 indicating different levels of the porous effect. When the porosity is small, the cylinders are very permeable, and when it is big, they can be treated almost like solid bodies. Hence, if the resistivity is 10000, the flow field should be similar to that of the solid case. This can be demonstrated in Fig. 6 where velocity magnitudes in three locations are plotted by using different orders of schemes. The results from the solid case is used as a benchmark solution for comparison. The results of 2nd–order upwind scheme appear to be a lot different from the results by using other schemes, especially in the bottom location where there are wiggles near the inlet, indicating highly unstable numerical results. The results obtained from 3rd-order upwind scheme and the 5th-order WENO schemes are close to each other. The high resistivity results show again that the 2nd-order upwind scheme should not be used. Since the interface behavior is the key issue in the fluid/porous interaction study, the surface pressure coefficient (C_p) distribution is used as the parameter for comparison. Figure 7 compares the C_p for the high-resistivity case around the center cylinder using different schemes along the solid cylinder case. The same conclusion is obtained from the results as that for the velocity profiles in Fig. 6 as discussed above.

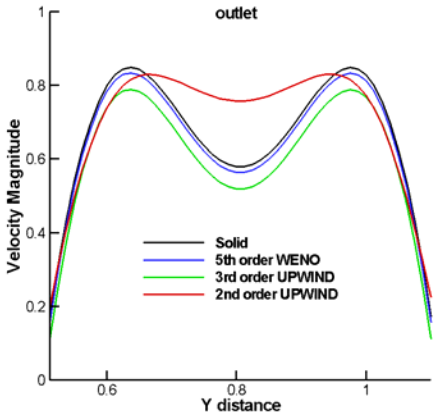

(a) outlet

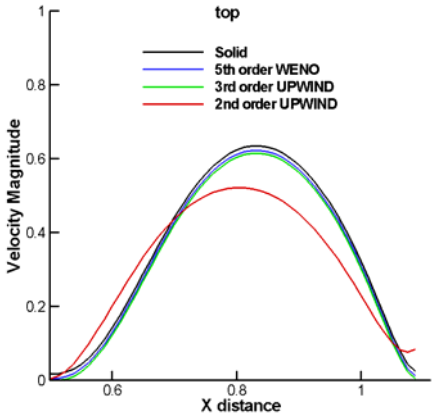

(b) top

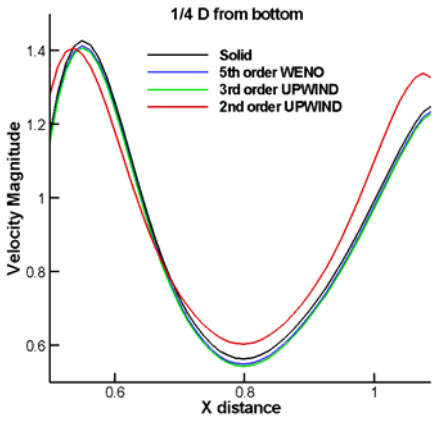

(c) bottom

Figure 6 Velocity profile comparisons for the porous cylinder case with $\sigma = 10000$: a) at the outlet; b) at the top boundary; c) 1/4 D from the bottom boundary.

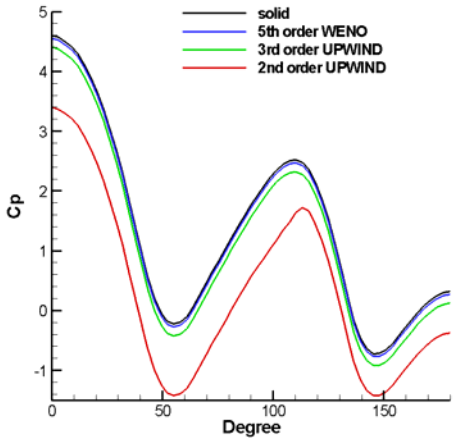

Figure 7 Porous cylinders unit: $\sigma = 10000$, pressure coefficient (C_p) comparison on the surface of the central cylinder

In the porous cylinder cases, when the flow resistivity is getting smaller, which means that the cylinders become more permeable, the differences between high-order schemes are more easily distinguished. In Fig. 8, the resistivity is 0.1, much smaller than the almost-solid case with $\sigma = 10000$. In the results from the 3rd–order upwind scheme, due to the numerical errors around the fluid/porous interfaces, the structures of the cylinders are almost indiscernible (Fig. 8a), which means the accuracy on the fluid/porous interfaces is not sufficient to resolve the boundaries. On the other hand, in Fig. 8(b) for the results of the 5th–order WENO scheme, the interfaces between the fluid and the porous cylinders are clearly shown, and the periodicity of the flow is well captured. Therefore, after all those tests, the 5th-order WENO scheme has been proved to be the one with the most accurate result. The above mentioned tests are summarized in Table 2.

	solid	$\sigma = 10000$	$\sigma = 0.1$
2nd-order central difference	X	X	X
2nd-order upwind	√	X	X
3rd-order upwind	√	√	X
5th-order WENO	√	√	√

Table 2 Summary of the numerical schemes used for testing (check means good results and cross means bad results)

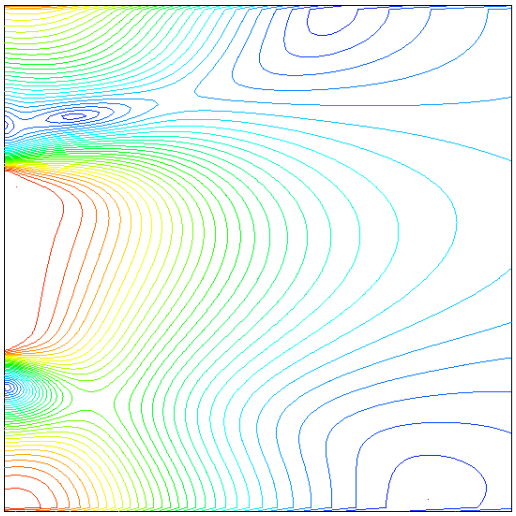

(a)

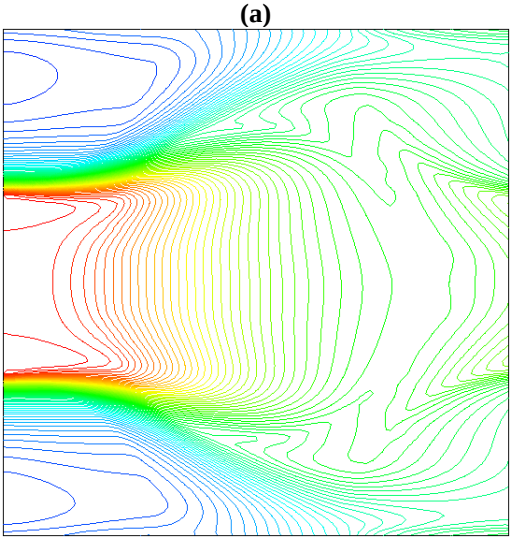

(b)

Figure 8 Velocity magnitude contours for the porous cylinders case with resistivity = 0.1: a) 3rd-order upwind scheme; b) 5th-order WENO scheme

After obtaining good results from the flow field for both solid and porous cylinder arrays, the species transport equation is then solved with the 5th-order WENO scheme using the solved flow field. As in Eq. (7), the porous model for the species sink term is only applied inside the porous cylinders. In the species transport equation, Eq. (6), the species diffusion coefficient, D_C, is selected as 0.001 for testing purposes. For the porous model in Eq. (7), the absorption coefficient varies from 0.01 to 10000 to test its effect on species transport. In Fig. 9, contours of species concentration are displayed with different absorption coefficient values. It shows for higher absorption coefficient, the species concentration in between cylinders is higher, while for lower absorption coefficient, the surface diffusion is more significant and there exist higher concentrations of species inside the cylinders.

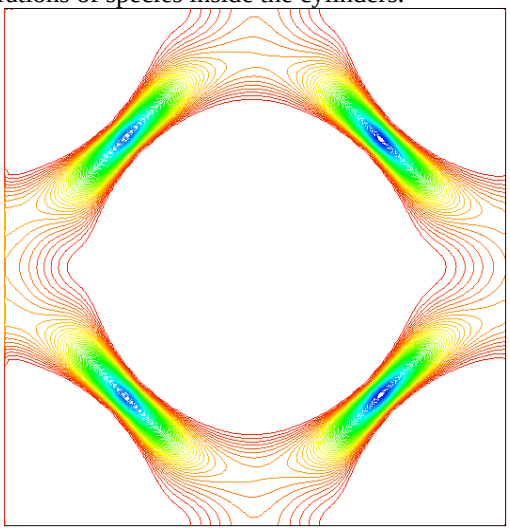

(a)

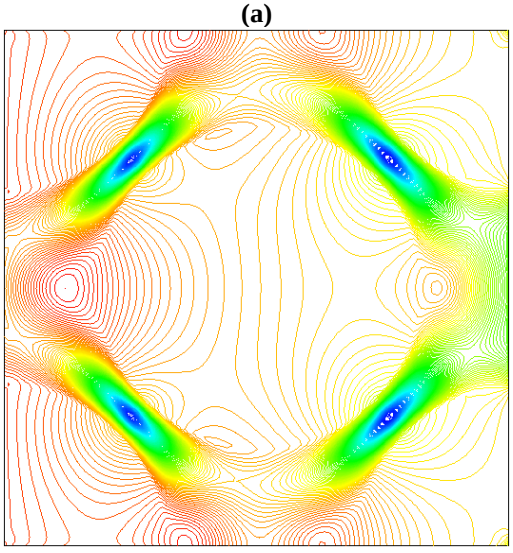

(b)

Figure 9 Species transport around porous cylinder arrays with different absorption coefficient: a) $\alpha = 10000$; b) $\alpha = 1$.

In a similar way that we found the correlation between the porosity (ϕ) and the pressure gradient (dp/dx) in the solid cylinder bundle system, in the porous case, a relationship between the adsorption coefficient (α) and the concentration change between the inlet and outlet (ΔC) is also anticipated. However, there has not been any empirical correlation for this problem like the Ergun equation for the momentum transport. To calculate the concentration change along the flow direction, an analogy of Eq. (17) is expressed as:

$$\Delta C = -\frac{1}{H - D/2} \int_{D/2}^{H-D/2} (C|_{x=0} - C|_{x=H}) dy \qquad (20)$$

To test the adsorption coefficient effect, a series of simulations of different α (0.01, 0.1, 1, 10, 100, 10000) are carried out with the same porous cylinder REV at $\phi = 0.609375$. Figure 10 plots the calculated concentration change correlated with adsorption coefficient. When the adsorption coefficient increases, the concentration change becomes less since there is less mass absorbed into the porous cylinders. However, the decrease of the concentration change does not linearly change with the absorption coefficeint.

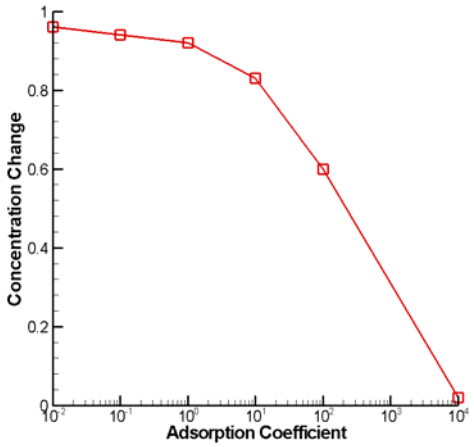

Figure 10 Effect of adsorption coefficient on concentration change

CONCLUSION

The paper presented a series of results from the numerical simulations for flow past a periodic array of both solid and porous cylinders. To maintain numerical accuracy on the interfaces between fluid and solid or porous cylinders, different orders of numerical schemes have been tested to discretize the momentum flux including the 2nd- and 3rd- order upwind schemes and the 5th-order WENO scheme. By using an REV

representing an array of impermeable solid cylinders, the present models with different high-order schemes are validated showing the 3rd-order upwind and the 5th-order WENO schemes are the more accurate schemes. The solid-cylinder REV results are used to compare with the Ergun equation for the bulk porous medium behavior. The results from the porous cylinders arrays with a range of flow resistivities showed that the 5th-order WENO scheme behaves the best from all the tests. The WENO scheme is then used to calculate the species transport with porous cylinder arrays. The results show that for the same geometric arrangement of the cylinder array and same species, the concentration distribution of the species is influenced by the absorption coefficient of the porous cylinders. The concentration change between the inlet and outlet decreases with the increase of the absorption coefficient.

ACKNOWLEDGMENTS

The support from Targeted Excellence Grant of Kansas State University is acknowledged.

REFERENCES

Bhattacharyya, S., Dhinakaran, S. and Khalili, A., 2006, "Fluid Motion around and through a Porous Cylinder," *Chem. Engr. Sci*, Vol. 61, pp. 4451-4461.

Chen, X. B., Yu, P., Winoto, S. H. and Low, H. T., 2008, "Numerical Analysis for the Flow past a Porous Square Cylinder based on the Stress-Jump Interfacial-Conditions," *Int. J. Numer. Method H.*, Vol. 18, pp. 635-655.

Chen, X. B., Yu, P., Winoto, S. H. and Low, H. T., 2009, "Numerical Analysis for the Flow past a Porous Trapezoidal-Cylinder based on the Stress-Jump Interfacial-Conditions," *Int. J. Numer. Method H.*, Vol. 19, pp. 223-241.

Cho, Y., Chopra, J. and Morris, P. J., 2007, "Immersed Boundary Method for Compressible High-Reynolds Number Viscous Flow around Moving Bodies," *45th AIAA Aerospace Sciences Meeting*, January 9-11, 2007, Reno, NV.

Ergun, S., 1952, "Fluid flow through packed columns," *Chem. Engr. Prog.*, Vol. 48, pp. 89-94.

Goyeau, B., Lhuillier, D., Gobin, D. and Velarde, M. G., 2003, "Momentum Transport at a Fluid-Porous Interface," *Int. J. Heat. Mass Tran.*, Vol. 46, pp. 4071-4081.

James, D. F. and Davis, A. M. J., 2001, "Flow at the Interface of a Model Fibrous Porous Medium," *J. Fluid Mech.*, Vol. 426, pp. 47-72.

Harten, A., Engquist, B., Osher, S. and Chakravarthy, S. R., 1987, "Uniformly High-Order Accurate Essentially Nonoscillatory Schemes .3," *J. Comp. Phys.*, Vol. 71, pp. 231-303.

Kuwahara, F., Kameyama, Y., Yamaashita S. and Nakayama A., 1998, "Numerical Modeling of Turbulent Flow in Porous Media Using a Spatially Periodic Array," *J. Porous Media*, Vol. 1, pp. 47-55.

Kuwahara, F., Yamane, I. and Nakayama, A., 2006, "Large Eddy Simulation of Turbulent Flow in Porous Media," *Int. Comm. Heat Mass Tran.*, Vol. 33, pp. 411-418.

Liang, C. and Papadakis, G., 2007, "Large Eddy Simulation of Cross-Flow through a Staggered Tube Bundle at Subcritical Reynolds Number," *J. Fluids Struct.*, Vol. 23, pp. 1215-1230.

Mittal, R. and Iaccarino, G., 2005, "Immersed Boundary Method," *Annu. Rev. Fluid. Mech.*, Vol. 37, pp. 239-261.

Moulinec, C., Pourquie, M., Boersma, B. J., Buchal, T. and Nieuwstadt, F. T. M., 2004, "Direct Numerical Simulation on a Cartesian Mesh of the Flow through a Tube Bundle," *Int. J. Comp. Fluid Dyn.*, Vol. 18, pp. 1-14.

Nakayama, A., Kuwahara, F. and Hayashi, T., 2004, "Numerical Modelling for Three-Dimensional Heat and Fluid Flow through a Bank of Cylinders in Yaw," *J. Fluid Mech.*, Vol. 498, pp. 139-159.

Ochoa-Tapia, J. A. and Whitaker, S., 1995, "Momentum Transfer at the Boundary between a Porous Medium and a Homogeneous Fluid 1: Theoretical Development," *Int. J. Heat. Mass Tran.*, Vol. 38, pp. 2635-2646.

Ochoa-Tapia, J. A. and Whitaker, S., 1995, "Momentum Transfer at the Boundary between a Porous Medium and a Homogeneous Fluid 2: Comparison with Experiment," *Int. J. Heat. Mass Tran.*, Vol. 38, pp. 2647-2655.

Papaioannou, G. V., Yue, D. K. P., Triantafyllou, M. S. and Karniadakis, G. E., 2006, "Evidence of Holes in the Arnold Tongues of Flow past Two Oscillating Cylinders," *Phys. Rev. Lett.*, Vol. 96, pp. 4-7.

Papaioannou, G. V., Yue, D. K. P., Triantafyllou, M. S. and Karniadakis, G. E., 2006, "Three-Dimensionality Effects in Flow around Two Tandem Cylinders," *J. Fluid Mech.*, Vol. 558, pp. 387-413.

Patankar, S. V., Liu, C. H. and Sparrow, E. M., 1977, "Fully Developed Flow and Heat-Transfer in Ducts Having Streamwise-Periodic Variations of Cross-Sectional Area," *J. Heat Trans.-T. ASME*, Vol. 99, pp. 180-186.

Pedras, M. H. J. and De Lemos, M. J. S., 2001, "Simulation of Turbulent Flow in Porous Media Using a Spatially Periodic Array and a Low Re Two-Equation Closure," *Numer. Meat Tr. A-Appl.*, Vol. 39, pp. 35-59.

Rollet-Miet, P., Laurence, D. and Ferziger, J., 1999, "LES and RANS of Turbulent Flow in Tube Bundles," *Int. J. Numer. Method H.*, Vol. 20, pp. 241-254.

Roychowdhury, D. G., Das, S. K. and Sundararajan, T., 2002, "Numerical Simulation of Laminar Flow and Heat Transfer

over Banks of Staggered Cylinders," *Int. J. Numer. Method H.*, Vol. 39, pp. 23-40.

Shu, C. W. and Osher, S., 1988, "Efficient Implementation of Essentially Non-Oscillatory Shock-Capturing Schemes," *J. Comp. Phys.*, Vol. 77, pp. 439-471.

Shu, C. W. and Osher, S., 1989, "Efficient Implementation of Essentially Non-Oscillatory Shock-Capturing Schemes .2," *J. Comp. Phys.*, Vol. 83, pp. 32-78.

Swarztrauber, P. N. and Sweet, R. A., 1979, "Algorithm 541: Efficient Fortran Subprograms for the Solution of Separable Elliptic Partial Differential Equations [D3]," *ACM T. Math. Software*, Vol. 5, pp. 352-364.

Teruel, F. E., 2007, *Macroscopic Turbulence Modeling and Simulation for Flow through Porous Media*, Ph.D. thesis, University of Illinois at Urbana-Champaign, Urbana-Champaign, IL.

Teruel, F. E. and Rizwan, U., 2009, "A New Turbulence Model for Porous Media Flows. Part I: Constitutive Equations and Model Closure," *Int. J. Heat. Mass Tran.*, Vol. 52, pp. 4264-4272.

Teruel, F. E. and Rizwan, U., 2009, "A New Turbulence Model for Porous Media Flows. Part I: Analysis and Validation Using Microscopic Simulations," *Int. J. Heat. Mass Tran.*, Vol. 52, pp. 5193-5203.

Teruel, F. E. and Rizwan, U., 2009, "Characterization of a Porous Medium Employing Numerical Tools: Permeability and Pressure-Drop from Darcy to Turbulence," *Int. J. Heat. Mass Tran.*, Vol. 52, pp. 5878-5888.

Williamson, C. H. K., 1996, "Vortex Dynamics in the Cylinder Wake," *Annu. Rev. Fluid. Mech.*, Vol. 28, pp. 477-539.

Wilson, D. K., Collier, S. L., Ostashev, V. E., Aldridge, D. F., Symon, N. P. and Marlin, D. H., 2006, "Time-domain modeling of the acoustic impedance of porous surfaces," *Acta Acustica United with Acustica*, Vol. 92, pp. 965-975.

Wilson, D. K., Ostashev, V. E., Collier, S. L., Symons, N. P., Aldridge, D. F. and Marlin, D. H., 2007, "Time-domain calculations of sound interactions with outdoor ground surfaces," *App. Acous.*, Vol. 68, pp. 173-200.

Xu, Y., Zheng, Z. C. and Wilson, D. K., 2010, "Simulation of Turbulent Wind Noise Reduction by Porous Windscreens Using High-order Schemes," *J. Comp. Acous.*, accepted.

Yang, X. and Zheng, Z. C., 2010, "Nonlinear Spacing and Frequency Effects of an Oscillating Cylinder in the Wake of a Stationary Cylinder," *Phys. Fluids*, Vol. 22, 043601.

Zdravkovich, M. M., 1997, Flow around Circular Cylinders, Oxford University Press.

Zhang, N. and Zheng, Z. C., 2007, "An Improved Direct-Forcing Immersed-Boundary Method for Finite Difference Applications," *J. Comp. Phys.*, Vol. 221, pp. 250-268.

Zwikker, C., and Kosten, C. W., 1949, *Sound Absorbing Materials*, Elsevier, New York.